Catalysis Today 252 (2015) 61–69

Catalysis Today

journal homepage: www.elsevier.com/locate/cattod

Microcontaminant degradation in municipal wastewater treatment plant secondary effluent by EDDS assisted photo-Fenton at near-neutral pH: An experimental design approach

S. Papoutsakis [b,d], S. Miralles-Cuevas [a], I. Oller [a,d], J.L. Garcia Sanchez [c], C. Pulgarin [b], S. Malato [a,d,*]

[a] Plataforma Solar de Almeria – CIEMAT, Carretera de Senés, km 4, 04200 Tabernas, Spain
[b] Ecole Polytechnique Fédérale de Lausanne, ISIC, Station 6, CH-1015 Lausanne, Switzerland
[c] Departamento de Ingeniería Química de la Universidad de Almería, Carretera Sacramento S/N, 04120 Almería, Spain
[d] CIESOL, Joint Centre of the University of Almería-CIEMAT, 04120 Almería, Spain

ARTICLE INFO

Article history:
Received 14 July 2014
Received in revised form 5 February 2015
Accepted 6 February 2015
Available online 28 February 2015

Keywords:
Advanced oxidation processes (AOP)
Iron complexes
Photo-Fenton
Municipal wastewater treatment

ABSTRACT

This work aims to evaluate the applicability of EDDS (ethylenediamine-N,N′-disuccinic acid) as an iron chelating agent for photo-Fenton treatment of municipal wastewater spiked with organic contaminants at near-neutral pH. A series of laboratory scale experiments are conducted under simulated sunlight in accordance with a central composite experimental design in order to define the most favorable conditions in terms of initial iron concentration (maintaining a molar ratio 1:2 of Fe:EDDS), H_2O_2 and pH. The system is evaluated in terms of degradation efficiency, H_2O_2 consumption and iron availability. The simulated system has been compared in terms of degradation efficiency with a 60 L compound parabolic collector (CPC), and significant correlation has been observed. An approach for estimating near-optimal regions of operability is also demonstrated.

1. Introduction

The inability of conventional wastewater treatment facilities to fully eliminate recalcitrant organic contaminants has been a source of growing concern in recent years. Compounds found in common household, agricultural or pharmaceutical products are found in wastewater plant effluent streams prior to release into the aquatic environment. Even though the concentrations in which they are found is usually in the ng to μg per liter scale, their continuous disposal unavoidably leads to accumulation in natural waters, provoking potential long-term health and ecological risks [1–3].

Advanced oxidation processes (AOPs) are a promising set of processes considered for application as part of tertiary treatment of effluents coming from municipal wastewater treatment plants (MWTP) [4–7]. Their capacity to generate highly reactive, non-selective reactive oxygen species (ROS), mainly HO• lead to the chemical elimination of biologically recalcitrant contaminants, increasing biodegradability of effluent streams. The Fenton process is an AOP, in which the production of ROS is driven by the iron mediated decomposition of H_2O_2, with the following reactions taking place in solution (React. 1):

$$Fe^{2+} + H_2O_2 \rightarrow Fe^{3+} + OH^- + HO^\bullet \quad (R1)$$

$$Fe^{3+} + H_2O_2 \rightarrow Fe^{2+} + HO_2^\bullet + H^+ \quad (R2)$$

$$HO^\bullet + H_2O_2 \rightarrow HO_2^\bullet + H_2O \quad (R3)$$

$$HO^\bullet + Fe^{2+} \rightarrow Fe^{3+}OH^- \quad (R4)$$

$$Fe^{3+} + HO_2^\bullet \rightarrow Fe^{2+} + O_2H^+ \quad (R5)$$

$$Fe^{2+} + HO_2^\bullet + H+ \rightarrow Fe^{3+} + H_2O_2 \quad (R6)$$

$$HO_2^\bullet + HO_2^\bullet \rightarrow H_2O_2 + O_2 \quad (R7)$$

As seen in (Reacts. 1–7), generation of hydroxyl and hydroperoxyl radicals is dependent on the cycling of iron between the Fe^{2+} and Fe^{3+} states. However, as (React. 1) is several orders of magnitude faster than (Reacts. 2–7), iron remains primarily as Fe^{3+}, effectively stopping the process.

In water, Fe^{3+} is subjected to extensive hydrolysis, forming different Fe^{3+}-aqua complexes depending on pH. At pH around 3, $[Fe(H_2O)_5(OH)]^{2+}$ is the predominant species, which exhibits significant photoactivity in the UV and visible region of solar radiation

* Corresponding author: Tel.: +34 950387940; fax: +34 950365015.
E-mail address: Sixto.malato@psa.es (S. Malato).

http://dx.doi.org/10.1016/j.cattod.2015.02.005
0920-5861/

[8] Under illumination, Fe^{2+} is regenerated in a variant called the photo-Fenton (React. 8)

$$[Fe(H_2O)_5(OH)]^{2+} + hv \rightarrow Fe^{2+} + H^+ + HO^\bullet \quad (R8)$$

The main limitation of the photo-Fenton process is the necessity to maintain the pH acidic throughout the treatment, as Fe^{3+}-aqua complexes tend to precipitate above pH 3 [9]. The acidified effluent also has to be neutralized before releasing to the environment. This introduces significant drawbacks in terms of reagent costs, operational complexity as well as the reduced quality of the treated water due to higher salt content.

The use of organic iron-complexing ligands has recently been gaining interest as a means of enhancing the performance of photo-Fenton photocatalytic systems [10]. Compared with Fe^{3+}-aqua complexes, Fe^{3+}-organic ligand complexes can maintain their solubility at a wider pH range, limiting the need for acidification and pH control. Additionally, many of them exhibit improved quantum yields, and photoactivity in a wider fraction of the solar spectrum, up to 580 nm. The generalized photo-Fenton reaction is presented below (React. 9)

$$Fe^{3+}\text{-}L + hv \rightarrow Fe^{2+}\text{-}(L)_{n-1} + L^\bullet \quad (R9)$$

Among the most well studied ligands are oxalic acid [11,12] and citric acid [13,14]. Although both are capable of maintaining iron soluble at neutral pH, the optimal behavior of Fe(III)-citrate and Fe(III)-oxalate photochemical processes are still under slightly acidic pH (5.0 for Fe(III)-citrate and 4.3 for Fe(III)-oxalate) [15,16]. Treatment of the near neutral MWTP effluent would therefore not be optimal. Additionally, the use of oxalic acid could introduce significant toxicity concerns [17]. The complex fraction of natural organic matter known as humic acids has also attracted some interest due to its ubiquitous presence in natural waters [18,19]. Treatment of heavily contaminated industrial wastewater has been shown to be efficient at neutral pH with the addition of humic acids [20]. However, for treating contaminants at the $\mu g\,L^{-1}$ level in neutral pH MWTP effluent, degradation rate was slow and the residual pH acidic, requiring adjustment prior to release [21].

Of particular interest are aminopolycarboxylic acids (APCAs), which can form stable water-soluble complexes over a wide pH range. Ethylenediaminetetraacetic acid (EDTA) has been extended in industrial applications due to its ability to solubilize and inactivate metal ions. However, due to its high biorecalcitrance, it has been classified as a persistent pollutant [22,23]. An alternative APCA, ethylenediamine-N,N′-disuccinic acid (EDDS) has metal complexing properties similar to EDTA, but is biodegradable and considered environmentally safe [24,25]. Due to these favorable characteristics, the use of EDDS is an attractive option for application in municipal wastewater tertiary treatments.

Previous work with EDDS in real MWTP effluents has been promising, demonstrating that the use of Fe:EDDS at 0.1:0.2 mM concentration ratio can efficiently degrade emerging contaminants at neutral pH [26,27]. However, a systematic study focusing on the effect of the common parameters affecting the photo-Fenton process applied at neutral pH and in the presence of EDDS has never been done.

The aim of this work is to better understand the effect of pH, H_2O_2 and Fe:EDDS concentrations on various aspects of an EDDS-assisted photo-Fenton treatment of MWTP effluents spiked with five micro-contaminants by performing a central composite experimental design (CCD). Phenol, bisphenol A, sulfamethoxazole, carbamazepine and pyrimethanil were chosen so as to be representative of the spectrum of different classes of chemicals commonly found in municipal wastewater. Response surfaces were constructed for initial degradation rate, percentage of contaminants degraded, H_2O_2 efficiency and stability of soluble iron. Lab-scale and pilot-scale systems were compared and an approach for determining operability regions of near-optimal performance was carried out.

Table 1
Composition of the MWTP effluents used in this work.

Main parameters	Range
Ions ($mg\,L^{-1}$)	
Cl^-	440–687
NO_2^-	3.5–4.0
Br^-	3.0–3.5
NO_3^-	3.0–4.5
SO_4^{2-}	148–174
Na^+	276–358
NH_4^+	19–50
K^+	26–35
Mg^{2+}	63–89
Ca^{2+}	78–114
Turbidity (NTU)	8.5–9.0
Conductivity ($mS\,cm^{-1}$)	1.9–2.1
pH	7.6–7.8
COD ($mg\,L^{-1}$)	60–62
IC ($mg\,L^{-1}$)	80–102
DOC ($mg\,L^{-1}$)	11–15

2. Materials and methods

2.1. Reagents

Iron source $Fe_2(SO_4)_3{\cdot}H_2O$ (75% purity) and (S,S)-ethylenediamine-N,N′-disuccinic acid trisodium salt solution (35% w/v) were both provided by Sigma–Aldrich. Hydrogen peroxide (30% w/v) was purchased from Pancreac. Sulfuric acid (96%) and sodium hydroxide were obtained from J.T. Baker. Carbamazepine and bisphenol A were obtained from Sigma–Aldrich. Sulfamethoxazole from Fluka, phenol from Pancreac and pyrimethanil from Agrevo. Acetonitrile (ACN) for the UPLC mobile phase was HPLC-grade and provided by Sigma–Aldrich. Millex PVDF 0.45 μm filters were used for the preparation of the UPLC samples. For dissolved organic carbon, dissolved iron and H_2O_2 analyses, Millipore Nylon 0.20 μm were used.

2.2. Municipal wastewater treatment plant effluent

All experiments were conducted in actual wastewater collected from the El Ejido (Almería, Spain) municipal wastewater treatment plant (MWTP), downstream of the secondary biological treatment. H_2SO_4 was used to strip HCO_3^-/CO_3^{2-} (measured as inorganic carbon (IC)), until the final IC load was below 5 $mg\,L^{-1}$ in order to avoid scavenger effect on hydroxyl radicals. Care was taken to significantly modify the natural water pH. Wastewater collected from the experimental design was stored under refrigeration (4–6 °C) and used within 10 days. Treated effluent collected from the pilot-scale experiments was used within 3 days. Some important physicochemical characteristics have been measured and can be seen in Table 1.

2.3. Analytical setup

The mixture of contaminants was prepared and stored in pure methanol, at a concentration of 1500 $mg\,L^{-1}$ each as the parent solution. When the contaminants were added to the effluent, a small amount of DOC from methanol (20 $mg\,L^{-1}$) was also introduced. An analytical method for Ultra Performance Liquid Chromatography (UPLC) has been developed. A Zorbax XDB-C18 column (4.6 × 50 mm, particle size 1.8 μ) was used. A linear gradient of 25 mM formic acid/ACN solutions was used, progressing from 80/20 to 0/100 in 8 min. Post time for subsequent equilibration was 4 min. The flow rate was 1 $mL\,min^{-1}$. UPLC samples were prepared

by filtering 8 mL of solution through a 0.45 μm PVDF syringe-driven filter, subsequently washed with 2 mL of ACN to verify total elution of the contaminants. The injected volume for all samples was 100 μL. The UV signal for each compound was recorded at the wavelength of maximum absorption (213 for phenol, 269 for carbamazepine, sulfamethoxazole and pyrimethanil, 280 for bisphenol A). Limits of detection (LOD) ranged from 1 to 7 $\mu g\,L^{-1}$, while limits of quantification (LOQ) ranged from 1.5 to 15 $\mu g\,L^{-1}$, depending on the contaminant. Concentrations were calculated using a 5-point calibration curve (5, 10, 25, 50 and 100 $\mu g\,L^{-1}$). Dissolved organic carbon (DOC) was measured by a Shimadzu TOC-V_{CSN} analyzer equipped with an ASI-V automatic sampler. Fe:EDDS complexes were prepared daily prior to the experiments by adding $Fe_2(SO_4)_3$ in 50 mL distilled water acidified at pH 3 and adding EDDS solution. Hydrogen peroxide concentrations were measured spectrophotometrically, by adding 0.5 mL of Titanium (IV) oxysulfate solution to 5 mL of sample and measuring absorbance at 410 nm (DIN 38402H15). Total dissolved iron concentration was measured by complexation with 1,10-phenanthroline and measuring absorbance at 510 nm (ISO 6332). All spectrophotometric measurements were made with a UNICAM UV/VIS spectrophotometer controlled with VISION software.

2.4. Experimental set-up and procedure

Experimental design was conducted in an Atlas XLS suntest solar simulator under constant illumination from a Xenon Lamp with an average UV irradiance of 30 $W\,m^{-2}$ (typical solar UV power during a sunny day). A cylindrical Pyrex glass vessel (height 8.5 cm, diameter 19 cm, wall thickness 3.2 mm) was filled with the MWTP effluent spiked with 100 $\mu g\,L^{-1}$ of each of the five contaminants (500 $\mu g\,L^{-1}$ of contaminants total) and the Fe:EDDS solution to a final volume of 1.5 L. This volume corresponds to a height of 5 cm in this vessel, deliberately chosen so as to be the same as the diameter of a CPC tube. The sides of the pyrex vessel were covered so that light could only penetrate to the upper surface (0.025 m^2 of illuminated area). UV radiation was monitored throughout the process with a SOLARLIGHT PMA2100 radiometer placed within the simulator. The pH was fixed to the desired level with 0.1 M solutions of NaOH or H_2SO_4. H_2O_2 was added and the simulator was sealed. Samples were taken every 5 min without disrupting the operation via a tube fixed to the vessel walls. The duration of each experiment was 60 min. pH was followed with a portable CRISON pH meter. Temperature was measured with a HANNA portable water resistant thermometer. All experiments were conducted at initial solution temperatures of 22 °C. Application of air cooling kept it below 29 °C during the course of the experiments.

Pilot scale experiments were conducted in a mobile CPC plant. The photocatalytic reactor was comprised of 20 borosilicate tubes (50 mm internal diameter, 1.5 m length, 2.5 mm thickness) and CPC mirrors of anodized aluminum. The plant was tilted 37°, equal to the local latitude (Tabernas, Almeria, Spain). Volume of each batch was 60 L, with an illuminated volume of 45 L and a total illuminated area of 4.5 m^2. Temperature and pH were monitored by probes inserted in the pipes. In all experiments the temperature never deviated from the 24–28 °C range, so its effect is assumed negligible. Wastewater was introduced into a recirculation tank then pumped into the tubes with a flow of 29 $L\,min^{-1}$ by using a centrifugal pump. Contaminants and Fe:EDDS were added and the pH was fixed with 2 M solutions of H_2SO_4/NaOH. H_2O_2 was then added and the system was left to recirculate. Solar photo-Fenton was initiated by uncovering the tubes and samples were taken every 5 min.

Accumulated energy (Eq. (1)) was used instead of treatment time in order to have a normalized value for comparing the efficiency between the two reactors of different size and geometry, including variations of solar irradiation during scaling-up experiments in the CPC pilot plant.

$$Q_{UV,n+1} = Q_{UV} + \Delta t_n \cdot \bar{UV}_{G,n+1} \cdot \frac{A_i}{V_T}; \qquad \Delta t_n = t_{n+1} - t_n; \tag{1}$$

where Q_{UV} ($kJ\,L^{-1}$) is the accumulated UV energy per unit of volume, $\bar{UV}_{G,n+1}$ ($W\,m^{-2}$) is the average solar ultraviolet radiation ($\lambda < 400$ nm) measured between t_{n+1} and t_n and A_i is the illuminated area (m^2). V_T (L) is the total volume of the reactor.

2.5. Central composite design

Response surface methodology (RSM) is a set of mathematical and statistical techniques widely used for analyzing engineering problems dependent on several variables. Central composite designs are among the most popular RSM methods, allowing for estimation of curvature along the response surface via the inclusion of quadratic terms. In this work, the chosen region of interest for each variable selected was between 0.025 and 0.25 mM for [Fe^{3+}] (Fe:EDDS always maintained at 1:2 ratio), [H_2O_2] between 30 and 100 $mg\,L^{-1}$ and pH between 5 and 8. Previous work has shown that 0.1:0.2 mM of Fe:EDDS has been sufficient for treating concentrations from 60 to1500 $\mu g\,L^{-1}$ of total contaminants in MWTP effluent with a H_2O_2 consumptions between 30 and 90 $mg\,L^{-1}$ [28]. The range of concentrations was chosen on the basis of these results. The choice of maintaining the molar ratio at 1:2 was made because it has been demonstrated to be favorable to 1:1 in terms of degradation rate and H_2O_2 consumption for the treatment of pharmaceuticals in MWTP effluent [27,28]. Higher ratios were not used in order to limit the increase of DOC due to the addition of EDDS. A rotatable central composite design with an alpha value of 1.682 would require experimentation at inadmissible negative values of Fe^{3+} concentration and pH values well beyond the typical ones found in real wastewater. In light of this limitation, a face-centered central composite design (FCD) was used instead, which is advisable whenever the regions of interest and operability coincide [29].

The experimental matrix found in Table 2 summarizes the performed runs. Minitab statistical software was used for analysis of the design and plotting of the response surfaces. Depiction of the response surfaces was made by holding one of the variables constant at the center point (5 for pH, 0.1375 mM for [Fe^{3+}] and 65 $mg\,L^{-1}$ for [H_2O_2]) and plotting the response as a function of the other two. A set of three graphs was generated for each response. Different responses have been selected in this study as it is explained below.

3. Results and discussion

When conducting an experimental design for an applied engineering problem, it can be worthwhile to explore multiple response factors. In this way, the effect of the operational variables on several aspects of the process can be evaluated. In this work, the following response factors have been studied, presented here along with their corresponding model equations (Eqs. (2)–(5)). Corresponding ANOVA tables for each model equation are presented in Table 3. Only the terms with $P < 0.1$ (90% level of significance) have been used for the construction of the model equations.

1) Initial degradation rate (in terms of $\mu g\,L^{-1}$ of contaminant removed per kJ of UV radiation received $R^2 = 0.9521$, F value of

Table 2
Experimental design matrix with each of the acquired responses ($R^2 > 0.990$ for the initial degradation rates used for the calculation of y_1).

Standard order	Run order	pH	Fe (mM)	H_2O_2 (mg L^{-1})	y_1 (μg kJ^{-1})	y_2 (%)	y_3 (μg/mg)	y_4 (%)
1	17	5.0	0.0250	30	195	31	4.2	22
2	4	8.0	0.0250	30	106	19	2.6	6
3	6	5.0	0.2500	100	1561	95	14.4	93
4	20	8.0	0.2500	30	610	67	8.1	91
5	14	5.0	0.0250	100	320	39	9.7	40
6	15	8.0	0.0250	100	118	17	2.0	5
7	18	5.0	0.2500	30	1283	80	11	90
8	3	8.0	0.2500	100	1230	93	6.6	75
9	8	5.0	0.1375	65	929	85	8.9	34
10	10	8.0	0.1375	65	464	70	4.8	40
11	7	6.5	0.0250	65	208	25	4.8	7
12	9	6.5	0.2500	65	804	90	7.2	92
13	11	6.5	0.1375	30	811	73	11.4	52
14	13	6.5	0.1375	100	826	92	9.6	30
15	2	6.5	0.1375	65	770	81	10.2	47
16	1	6.5	0.1375	65	801	79	9.9	49
17	5	6.5	0.1375	65	829	80	10.2	51
18	16	6.5	0.1375	65	814	80	11.4	48
19	12	6.5	0.1375	65	799	81	11.2	45
20	19	6.5	0.1375	65	819	82	10.4	48

model = 43.49):

$$y_1 = -279 + 163\text{pH} + 13096\text{Fe} - 6.86\text{H}_2\text{O}_2 - 17304(\text{Fe})^2 + 0.08(\text{H}_2\text{O}_2)^2 - 830\text{pH} \times \text{Fe} \quad (2)$$

2) Percentage of the sum of micro contaminants removed by the time the degradation process slows down ($R^2 = 0.9852$, F value of model = 136.51):

$$y_2 = -10.60 + 13.51\text{pH} + 598.54\text{Fe} - 0.14\text{H}_2\text{O}_2 - 1850(\text{Fe})^2 - 14.8\text{pH} \times \text{Fe} + 1.1\text{Fe} \times \text{H}_2\text{O}_2 \quad (3)$$

3) Efficiency of hydrogen peroxide consumption (in terms of μg L^{-1} of contaminant eliminated per mg L^{-1} of H_2O_2 consumed, $R^2 = 0.9054$, F value of model = 11.89):

$$y_3 = -26.21 + 11\text{pH} + 90.2\text{Fe} - 0.93(\text{pH})^2 - 0.36\text{Fe} \times \text{H}_2\text{O}_2 \quad (4)$$

4) Percentage of total dissolved iron in solution by the end of the process ($R^2 = 0.9686$, F value of model = 33.64):

$$y_4 = -40.52 + 19.80\text{pH} + 78\text{Fe} + 0.18\text{H}_2\text{O}_2 + 593(\text{Fe})^2 \quad (5)$$

3.1. Initial degradation rate (r_o) and percentage of degradation achieved

In Fig. 1 the response surfaces obtained for the two first response factors (y_1 and y_2) considered in this work are shown.

The Fe(III)-EDDS complex, if kept in the dark, is stable in the entirety of the 5–8 pH region. Due to the stability of the complex, iron is not initially available for participating in homogeneous Fenton reactions. No contaminant degradation was therefore observed in the dark, it was not available for participation in homogeneous Fenton reactions. Under illumination, the complex is rapidly photodegraded and the iron consequently liberated. Complete photodegradation of 0.1 mM of Fe(III)-EDDS has been reported to occur within only 12 min of UV–vis light (300 nm < λ < 500 nm) irradiation [30]. The low degradation efficiency observed when 0.025:0.05 mM of Fe:EDDS were used is indicative of the loss of iron from the solution. Higher Fe:EDDS concentrations would be more successful.

Initial degradation rate exhibits a downward trend between pH 5 and 8, regardless of H_2O_2 concentration. This behavior appears contrary to what has appeared in the literature (in demineralized water), where higher pH leads to higher initial rates when EDDS complex agent is used [31]. There are several effects which can occur within this pH range: first, at higher pH, superoxide radical anion ($O_2^{\bullet -}$) is present in higher quantities and contributes to the direction of the Fe(II)/Fe(III) equilibrium toward Fe(II) formation. Second, starting from pH 7 upwards, the speciation of Fe(III)/EDDS complexes begins to differ, with the form FeL^- decreasing and $FeOHL^{2-}$ becoming more dominant. At pH 8, it is suggested [30] that the two species are present in almost equal concentrations. As the $FeOHL^{2-}$ form is suggested to be less photochemically efficient [30], it could contribute to the decrease in degradation rate. Third, the quantum yield of $HO^{\bullet}$ formation from the photolysis of Fe(III)-EDDS increases at higher pH [31] (contrary to what happens with citrate, oxalate and Fe(III)-aqua complexes, whose quantum yield becomes negligible around pH 7 [32]). Fourth, the iron released once the Fe(III)-EDDS complex begins to photolyse would be expected to precipitate faster at higher pH, hindering the degradation. The fact that the initial rate is lower with increasing pH may mean that the equilibrium of these different elements in MWTP effluent is different than in demineralised water.

In addition, independently of the other two variables, there is not a significant influence of hydrogen peroxide on the initial degradation rate. As the entire range of H_2O_2 concentrations studied was about 2 orders of magnitude greater than of the contaminants, this result is not unexpected, especially given the complexity of the effluent.

Regarding the percentage of contaminants eliminated at the end of the process, it can be seen that at the lowest iron concentration (0.025 mM), removal percentage is lower than 40%, regardless of the combination of the other two variables. It could be argued however that the limiting step is the rapid photodegradation of the Fe(III):EDDS complex. The relatively low concentration of excess EDDS (0.05 mM total) recomplexes the iron in solution, but is depleted before complete degradation can be achieved. Studies conducted with varying ratios of Fe to EDDS have shown [33] that iron concentrations as low as 0.01 mM can be maintained in solution and contribute to contaminant degradation, provided EDDS is found in abundance (0.25 mM).

The influence of the pH on the percentage of contaminants degraded is relatively minimal throughout the whole region of interest. High pH may negatively affect the kinetics of the degradation, but the end-point nevertheless remains the same. This observed stability could be attributed, as mentioned above,

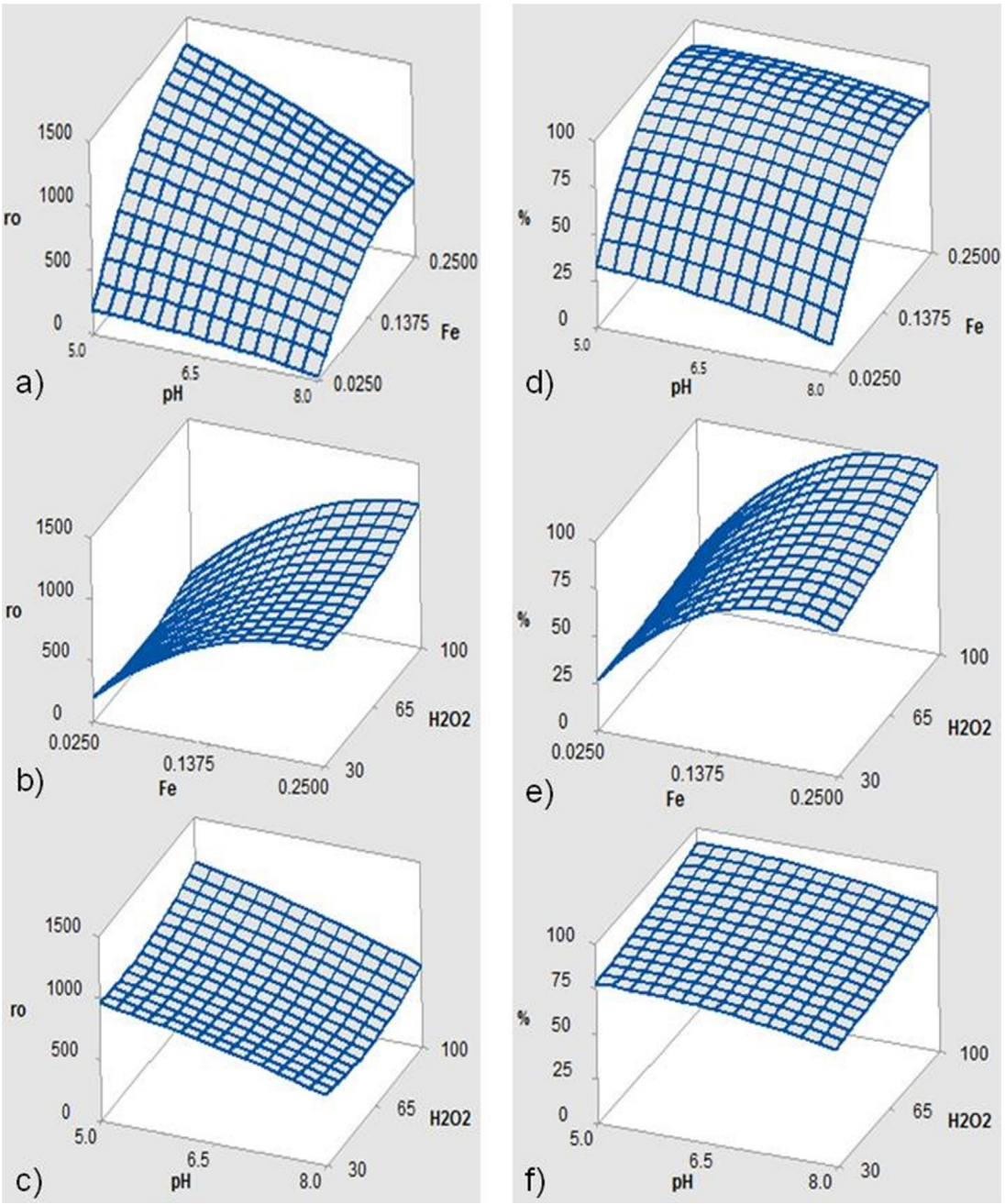

Fig. 1. Initial degradation rate (a–c) and percentage of contaminants removed by the end of the process (d–f). Factors kept constant: (a, d) [H_2O_2] 65 mg L^{-1}; (b, e) pH 6.5; (c, f) [Fe:EDDS] 0.1375:0.275 mM.

to the competing tendencies at higher pH between faster iron precipitation and higher quantum yield. Even though 30 mg L^{-1} of H_2O_2 are successful in removing about 70–75% of contaminants under all conditions, removal of 90% and above requires addition of H_2O_2 concentrations above 65 mg L^{-1}.

3.2. H_2O_2 consumption efficiency (R_p) and iron availability

In Fig. 2 the response surfaces obtained for the third and fourth response factors (y_3 and y_4) are shown.

H_2O_2 consumption efficiency (R_p = μg contaminant/mg H_2O_2 consumed) is exceptionally low at the lowest iron concentrations (Fig. 2(a and b)). As the concentration of EDDS is also low, its complete photodegradation occurs within a few minutes. The medium is almost immediately deprived of the decomplexed iron due to its fast precipitation (faster at higher pH values, Fig. 2(a)). In the absence of iron, it is probable that H_2O_2 is being consumed while reacting with the less recalcitrant natural organic compounds present in the wastewater.

Higher iron concentration allows for better H_2O_2 consumption, regardless of initial H_2O_2 concentration, and near-optimal values are clearly observed around 0.1375 mM.

Maintaining iron in solution is one of the most significant challenges when working at neutral pH. Therefore, it was of interest to observe its stability in the studied region. Fig. 2(d–f), displays the response surfaces of the percentage of iron remaining in solution after 60 min of simulated solar irradiation. Given the constant lamp radiation of 30 W m^{-2} of UVA, this corresponds to an accumulated UVA energy of 2.04 kJ L^{-1}. As seen in Fig. 2(d and e), almost all of the iron was lost at the lowest concentrations. The percentage of

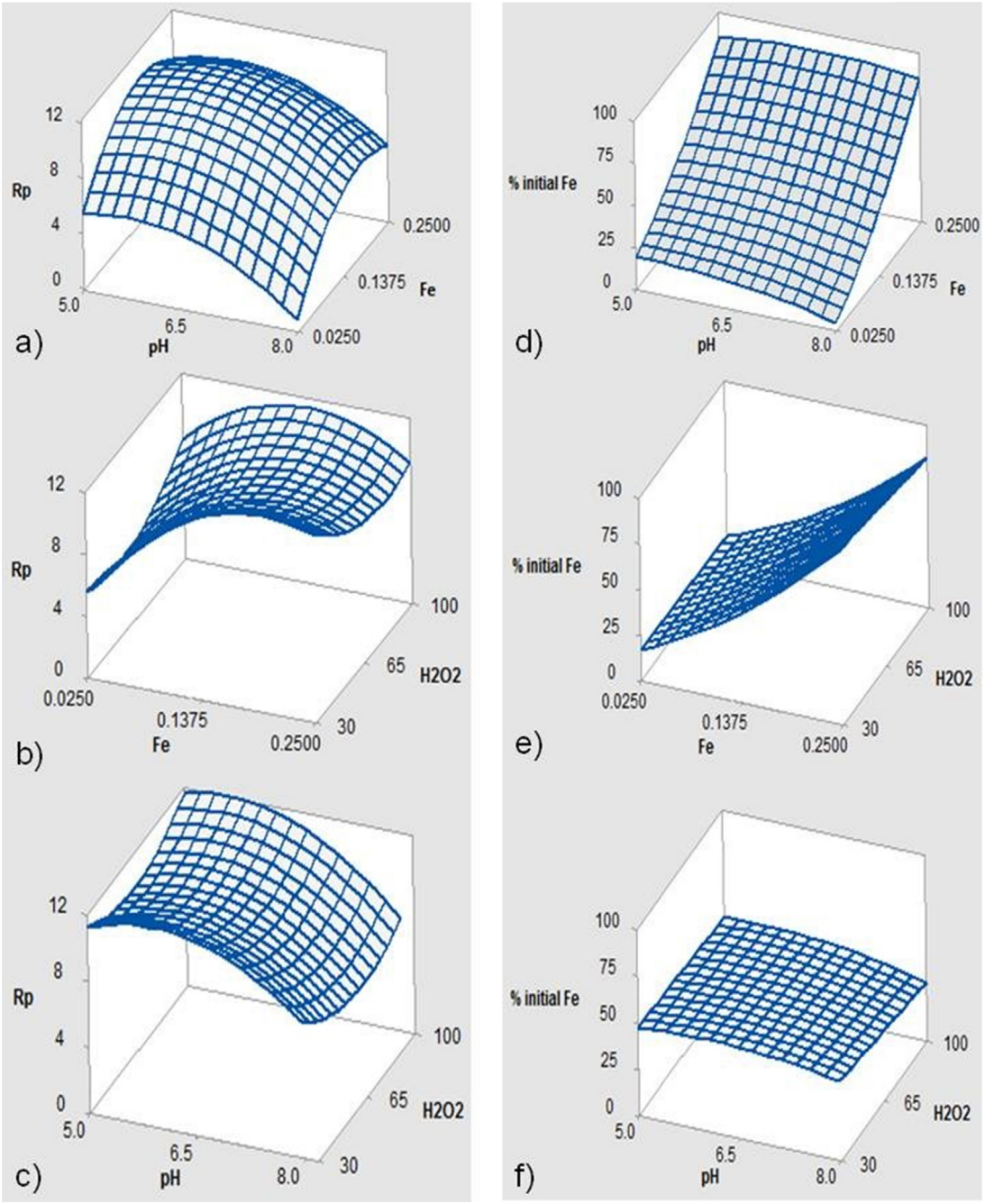

Fig. 2. H_2O_2 consumption efficiency (R_p, a–c) and soluble iron availability by the end of the process (d–f). Factors kept constant: (a, d) [H_2O_2] 65 mg L^{-1}; (b, e) pH 6.5; (c, f) [Fe:EDDS] 0.1375:0.275 mM.

iron remaining in solution increased with higher initial Fe:EDDS concentrations, with almost no losses observed at the highest concentrations. It is mentioned in the literature that the ratio between Fe(III) and EDDS in Fe(III)-EDDS species prevalent between pH 5 and 8 is always 1:1 [30]. Additionally, Metsarinne et al. [34] mentioned that while Fe(III)-EDDS is rapidly photodegraded, EDDS alone can be stable for days in both distilled and more complex lake water. Uncomplexed EDDS can thus be expected to remain stable for the duration of the experiment. Following the initial photochemical reaction, oxidation of Fe(II) and complexation has been suggested to be possible when EDDS is found in excess [33], according to the following reactions (Reacts. 3 and 4).

$$\mathrm{Fe(III)-EDDS} \xrightarrow{h\nu} [\mathrm{Fe(III)-EDDS}]* \rightarrow \mathrm{Fe(II)} + \mathrm{EDDS}^{\bullet} \quad \text{(R10)}$$

$$\mathrm{Fe(II)} + \mathrm{EDDS} \xrightarrow{O_2, H_2O_2} [\mathrm{Fe(III)-EDDS}] \quad \text{(R11)}$$

It should be mentioned that the observed loss of iron was not gradual from the beginning of the experiment but would happen rapidly from the moment a certain amount of radiation had been received by the system. At the highest concentrations (around 0.25:0.5 mM of Fe:EDDS), no loss of iron was observed at all during the 60 min of the experiment. Given that Fe(III)-EDDS photolysis begins almost immediately and that any free iron would be expected to precipitate rapidly in the 5–8 pH range, this delay seems to suggest that (React. 4) does indeed happen. The persistence of iron in solution at the highest Fe:EDDS concentrations also suggests that the complexation of free iron with excess EDDS was faster than its precipitation. In the case of medium concentrations,

Table 3
ANOVA tables for the linear, quadratic and interaction terms of each of the four model equations y_1 (a), y_2 (b), y_3 (c) and y_4 (d).

	DF	Adj SS	Adj MS	*F*-value	*P*-value
a)					
Model	9	2583051	287006	42.5	0
Linear	3	2220177	740059	110	0
pH	1	469589	469589	69.5	0
Fe	1	1709244	1709244	253	0
H_2O_2	1	41345	41345	6.1	0.033
Square	3	186448	62149	9.2	0.003
pH × pH	1	2259	2259	0.3	0.576
Fe × Fe	1	131904	131904	19.5	0.001
$H_2O_2 \times H_2O_2$	1	23959	23959	3.6	0.089
2-Way interactions	3	176425	58808	8.7	0.004
pH × Fe	1	156800	156800	23.2	0.001
pH × H_2O_2	1	3961	3961	0.59	0.462
Fe × H_2O_2	1	15664	15664	2.32	0.159
b)					
Model	9	12676.2	1408.5	136.1	0
Linear	3	9430.7	3143.6	303.6	0
pH	1	396.9	396.9	38.3	0
Fe	1	8584.9	8585.9	829.2	0
H_2O_2	1	448.9	449.9	43.4	0
Square	3	3033.5	1011.2	97.7	0
pH × pH	1	32	32	3.1	0.109
Fe × Fe	1	150	1507	145.6	0
$H_2O_2 \times H_2O_2$	1	7	7	0.7	0.431
2-Way interactions	3	212	70.7	6.8	0.009
pH × Fe	1	50	50	4.8	0.053
pH × H_2O_2	1	0	0	0	1
Fe × H_2O_2	1	162	162	15.6	0.003
c)					
Model	9	162	18	7.5	0.002
Linear	3	79.3	26	11	0.002
pH	1	39.5	39	16.6	0.002
Fe	1	39.1	39	16.4	0.002
H_2O_2	1	0.6	0.6	0.3	0.627
Square	3	66.2	22.1	9.2	0.003
pH × pH	1	11.9	11.9	5	0.049
Fe × Fe	1	23.5	23.5	9.8	0.011
$H_2O_2 \times H_2O_2$	1	6.8	6.8	2.9	0.122
2-Way interactions	3	16.5	5.5	2.3	0.139
pH × Fe	1	0.9	0.9	0.4	0.555
pH × H_2O_2	1	1.6	1.6	0.6	0.438
Fe × H_2O_2	1	14.1	14.1	5.9	0.036
d)					
Model	9	13929.4	1547.7	33.6	0
Linear	3	13569.8	4523.3	98.1	0
pH	1	152.1	152.1	3.3	0.099
Fe	1	13249.6	13249.6	287.3	0
H_2O_2	1	168.1	168.1	3.6	0.085
Square	3	181.3	60.4	1.3	0.325
pH × pH	1	44	44	0.9	0.352
Fe × Fe	1	154.7	154.7	3.3	0.097
$H_2O_2 \times H_2O_2$	1	0	0	0	1
2-Way interactions	3	178.4	59.5	1.3	0.331
pH × Fe	1	91.1	91.1	2	0.19
pH × H_2O_2	1	21.1	21.1	0.5	0.514
Fe × H_2O_2	1	66.1	66.1	1.4	0.259

the observed behavior means that only part of the excess EDDS was photodegraded within the time of the experiment and was available for complexing more iron through (React. 4).

Effects of pH and H_2O_2 on the percentage of iron retained in solution are minimal, although the curvature observed around pH 6.5 seems to be in accordance with Metsarinne et al. [34], who have observed higher stability of Fe(III)-EDDS at pH 6.5 both in distilled and lake water.

3.3. Scale-up to a CPC solar photo-reactor at pilot plant scale

In order to verify the general applicability of the results obtained in the solar simulator, a set of three conditions has been tested in a 60 L CPC photo-reactor under solar light.

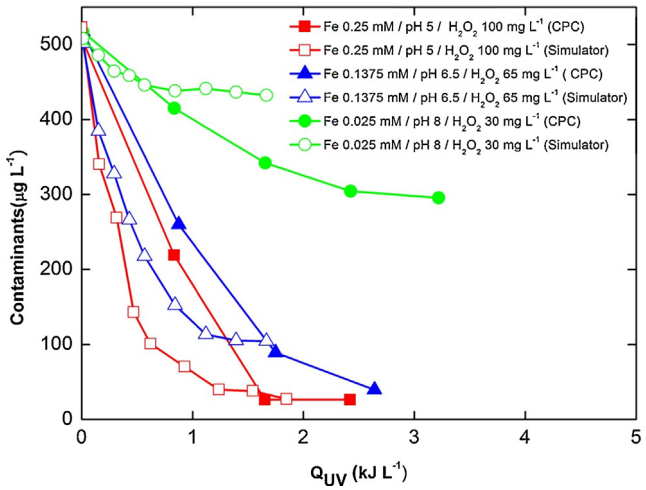

Fig. 3. Cross-scale comparison between the degradation performance on the 1.5 L photo-reactor under simulated solar radiation and using 60 L solar CPC pilot plant.

The rate of energy accumulation in the CPC tubes was higher than in the solar simulated system considering an average radiation of 30 W m^{-2} (about 0.17 kJ min^{-1} L^{-1} in the CPC compared to 0.03 kJ min^{-1} L^{-1} in the simulator), so the process was significantly faster. 90% degradation was reached in 35 min in the simulated system, while the same percentage was reached in the CPC in less than 10 min. As can be seen in Fig. 3, there is a good degree of correlation between the two systems despite the different timeframes. This correlation emphasizes the importance of UV energy density on degradation kinetics, independently of reaction volume. At low concentrations of Fe:EDDS the correlation was not adequate, as the system was most seriously affected by the loss of iron. As commented before, Fe (III)-EDDS photolysis begins almost immediately, releasing free iron that is expected to precipitate rapidly in the 5–8 pH range. The released iron cannot remain in solution for as long as required by the slower treatment in the solar simulator (as incident radiation per minute and liter was lower), so the process is hindered more seriously than in the CPC. This reinforces the idea that solar photo-reactors should be designed to profit the most of solar irradiation absorbance, maximizing illuminated volume/total volume ratio.

3.4. Desirability function approach for multiple response process optimization

When discussing optimization, it should be preferable to take into account more than one aspect of the process, seeking instead a compromise for achieving efficiency across multiple responses. This approach can help in defining regions of near-optimal performance. As there is a high degree of correlation in terms of accumulated Q_{UV} between the two systems, the experimental design results could be applied even in the context of multiple-module CPC reactor systems. In this case, the objective should be a set of condition achieving high initial degradation rate (y_1), complete contaminants removal (y_2) and high H_2O_2 consumption efficiency (y_3). A common strategy used within the response surface framework is the desirability function approach, consisting of converting the multiple responses into a single composite function [35]. For each of the three responses y_1, y_2, y_3, individual desirability functions (d_i) are defined according to Eq. (6). It can obtain values between 0 and 1, with maximum desirability obtained at the

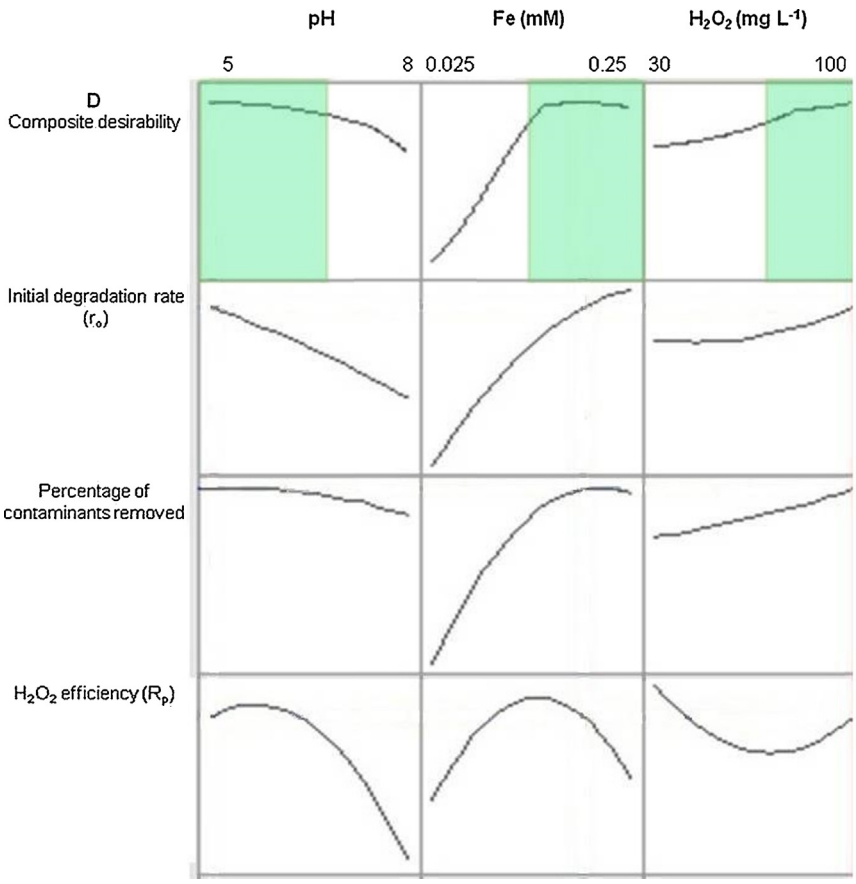

Fig. 4. Effect of initial pH, [H_2O_2] and [Fe] on composite desirability (row 1), initial degradation rate (row 2), percentage of contaminants removed (row 3) and H_2O_2 efficiency (row 4).

maximum response.

$$d_i = \begin{cases} 0 & y \le y_{\min} \\ \left(\dfrac{y - y_{\min}}{y_{\max} - y_{\min}}\right)^{W_i} & \\ 1 & y \ge y_{\max} \end{cases} \quad (6)$$

The parameter W_i represents a weight which defines the shape of the function. Large weights signify a sharp increase in d_i only when y_i is close to y_{max}. Consequently, if one of the responses has higher importance for a given optimization objective, setting a high W_i limits the acceptable range to a region very near the maximum. As reaching complete contaminant removal is the most important objective, the corresponding W_2 has been set higher than both W_1 and W_3. W_1 and W_3 have been set to 1, while W_2 has been set to 2.

An aggregate composite desirability function D is constructed by calculating the weighted geometric mean of the three individual desirabilities.

$$D = \sqrt[3]{{d_1}^{w_1} \times {d_2}^{w_2} \times {d_3}^{w_3}} \quad (7)$$

Each column of the plot shown in Fig. 4 displays the influence of each factor on the composite desirability D (row 1) and on each of the chosen responses (rows 2–4). Highlighted areas in Fig. 4 demonstrate acceptable operability conditions. In terms of process control, it could be said that pH would only have to be regulated when it strongly deviates toward high values. [Fe] should be around 0.2 mM, while [H_2O_2] should be above 65–70 mg L^{-1} for maximum removal. The chosen weights are indicative, as this approach allows for flexible optimization objectives, depending on individual priorities.

4. Conclusions

This work has verified that treatment of micro-contaminants with the use of EDDS as an iron-complexing agent is possible in real wastewater effluent at a pH range between 5 and 8. Initial degradation rate decreases at higher pH, but complete degradation is nevertheless achieved in the presence of sufficient Fe:EDDS concentrations. The fact that the contaminants are eliminated in the presence of relatively high DOC values (about 2 orders of magnitude greater) is especially promising.

The results obtained from the solar simulator provide a very good estimate of the behavior of the pilot-scale CPC solar photoreactor in terms of Q_{UV}. Due to the limited irradiated area of the reactor in the solar simulator, the process was significantly longer. In the CPC however, the amount of radiation necessary for achieving complete degradation was reached within just a few minutes.

A correlation has also been made between iron precipitation and accumulated UV radiation. Further research is definitely required but it could allow for an empirical estimation of optimal Fe:EDDS ratios with respect to different applications.

References

[1] R. Loos, R. Carvalho, D.C. Antonio, S. Comero, G. Locoro, S. Tavazzi, B. Paracchini, M. Ghiani, T. Lettieri, L. Blaha, B. Jarosova, S. Voorspoels, K. Servaes, P. Haglund, J. Fick, R.H. Lindberg, D. Schwesig, B.M. Gawlik, Water Res. 47 (2013) 6475–6487.
[2] B. Petrie, R. Barden, B. Kasprzyk-Hordern, Water Res. (2014).
[3] J.-J. Jiang, C.-L. Lee, M.-D. Fang, Mar. Pollut. Bull. 85 (2014) 391–399.
[4] R. Rosal, A. Rodríguez, J.A. Perdigón-Melón, M. Mezcua, M.D. Hernando, P. León, E. García-Calvo, A. Agüera, A.R. Fernández-Alba, Water Res. 42 (2008) 3719–3728.
[5] N. De la Cruz, J. Giménez, S. Esplugas, D. Grandjean, L.F. de Alencastro, C. Pulgarín, Water Res. 46 (2012) 1947–1957.

[6] I. Oller, S. Malato, J.A. Sanchez-Perez, Sci. Total Environ. 409 (2011) 4141–4166.
[7] I. Michael, L. Rizzo, C.S. McArdell, C.M. Manaia, C. Merlin, T. Schwartz, C. Dagot, D. Fatta-Kassinos, Water Res. 47 (2013) 957–995.
[8] H. Gallard, J. De Laat, B. Legube, Water Res. 33 (1999) 2929–2936.
[9] J.J. Pignatello, E. Oliveros, A. MacKay, Crit. Rev. Environ. Sci. Technol. 36 (2006) 1–84.
[10] B.M. Souza, M.W.C. Dezotti, R.A.R. Boaventura, V.J.P. Vilar, Chem. Eng. J. 256 (2014) 448–457.
[11] D.R. Manenti, P.A. Soares, A.N. Módenes, F.R. Espinoza-Quiñones, R.A.R. Boaventura, R. Bergamasco, V.J.P. Vilar, Chem. Eng. J. 266 (2015) 203–212.
[12] H. Nakagawa, E. Yamaguchi, Chemosphere 88 (2012) 183–187.
[13] H.B. Abrahamson, A.B. Rezvani, J.G. Brushmiller, Inorg. Chim. Acta 226 (1994) 117–127.
[14] J. Guo, Y. Du, Y. Lan, J. Mao, J. Hazard. Mater. 186 (2011) 2083–2088.
[15] Y. Chen, Z. Liu, Z. Wang, M. Xue, X. Zhu, T. Tao, J. Hazard. Mater. 194 (2011) 202–208.
[16] G. Liu, S. Zheng, X. Xing, Y. Li, D. Yin, Y. Ding, W. Pang, Chemosphere 78 (2010) 402–408.
[17] M.M. Rahman, R.B. Abdullah, W.E. Wan Khadijah, J. Anim. Physiol. Anim. Nutr. 97 (2013) 605–614.
[18] M.J. Farré, X. Doménech, J. Peral, J. Hazard. Mater. 147 (2007) 167–174.
[19] M. Kępczyński, A. Czosnyka, M. Nowakowska, J. Photochem. Photobiol. A: Chem. 185 (2007) 198–205.
[20] E. Lipczynska-Kochany, J. Kochany, Chemosphere 73 (2008) 745–750.
[21] N. Klamerth, S. Malato, M.I. Maldonado, A. Agüera, A. Fernández-Alba, Catal. Today 161 (2011) 241–246.
[22] Z. Yuan, J. Van Briesen, Environ. Eng. Sci. (2006) 533–544.
[23] C.K. Schmidt, M. Fleig, F. Sacher, H.J. Brauch, Environ. Pollut. 131 (2004) 107–124.
[24] A. Rastogi, S.R. Al-Abed, D.D. Dionysiou, Water Res. 43 (2009) 684–694.
[25] N.J. Velupula, G.J. Tedros, M.C. Andrew, Anal. Sci. 23 (2007) 493–496.
[26] N. Klamerth, S. Malato Rodríguez, A. Aguera, A. Fernández-Alba, Water Res. (2013) 833–840.
[27] S. Miralles-Cuevas, I. Oller, J.A.S. Pérez, S. Malato, Water Res. (2014).
[28] N. Klamerth, S. Malato, A. Aguera, A. Fernandez-Alba, G. Mailhot, Environ. Sci. Technol. 46 (2012) 2885–2892.
[29] P.J. Whitcomb, M.J. Anderson, Productivity Press, 2004.
[30] Y. Wu, M. Brigante, W. Dong, P. de Sainte-Claire, G. Mailhot, J. Phys. Chem. A 118 (2014) 396–403.
[31] W. Huang, M. Brigante, F. Wu, C. Mousty, K. Hanna, G. Mailhot, Environ. Sci. Technol. 47 (2013) 1952–1959.
[32] W. Huang, M. Brigante, F. Wu, K. Hanna, G. Mailhot, J. Photochem. Photobiol. A: Chem. (2012) 17–23.
[33] J. Li, G. Mailhot, F. Wu, N. Deng, J. Photochem. Photobiol. A: Chem. (2010) 1–7.
[34] S. Metsarinne, T. Tuhkanen, R. Aksela, Chemosphere (2001) 949–955.
[35] N.R. Costa, J. Lourenço, Z.L. Pereira, Chemom. Intell. Lab. Syst. 107 (2011) 234–244.